PERGAMON

AE International – North America

Atmospheric Environment 37 (2003) 1489–1502

ATMOSPHERIC ENVIRONMENT

www.elsevier.com/locate/atmosenv

# Using back trajectories and process analysis to investigate photochemical ozone production in the Puget Sound region

Guangfeng Jiang, Brian Lamb*, Hal Westberg

*Department of Civil and Environmental Engineering, Laboratory for Atmospheric Research, Washington State University, Pullman, WA 99164-2910, USA*

Received 9 June 2002; accepted 30 November 2002

**Abstract**

A photochemical Eulerian grid modeling system, consisting of MM5/CALMET/CALGRID, was modified to include a process analysis scheme, and a back trajectory method using the CALPUFF model in a reverse diffusion mode was implemented to define the air mass transport path reaching a downwind receptor from urban Seattle, WA. Process analysis was used to determine the relative importance of chemical production, advection, diffusion and deposition within the receptor grid cell and also along the air mass transport path from the urban source area to the receptor. This analysis was applied to an ozone episode occurring during 11–14 July 1996, in the Puget Sound region of Washington State. Within the receptor grid, the process analysis showed that ozone concentrations increase during the day as chemical production exceeds the net effects of deposition and vertical diffusion. Concentrations decrease after mid-afternoon when horizontal advection begins to dominate the other processes. When applied along the air mass transport path, process analysis shows that during most of the day, chemical production is larger than the other processes and causes the air mass ozone concentration to steadily increase during transport downwind of the urban core. Maximum ozone production rates equaled 20–25 ppb/h along the trajectory to the rural monitoring site where peak ozone levels occurred approximately 40 km downwind of urban Seattle, WA. The chemical production rates during this ozone evolution process play an important role in the peak ozone values. Higher peak ozone concentrations that occurred on Sunday, 14 July 1996 (118 ppbv), compared to those on Friday, 12 July 1996 (80 ppbv), were due, in part, to the higher ozone production rates along the trajectory to the rural monitoring site on 14 July compared to 12 July. These differences in chemical production appear to be related to differences in VOC/$NO_x$ ratios within the urban air mass for each day. The importance of VOC/$NO_x$ effects on the 2 days versus differences in meteorology was confirmed by running the simulation for Friday with Sunday emissions and using Sunday meteorological fields with Friday emissions. Differences in emissions for the 2 days produced almost twice the effect on peak ozone concentrations at the downwind receptor compared to the effects of differences in meteorology for these 2 days.


*Keywords:* Urban ozone; $NO_x$; VOC; Emissions; Washington state

## 1. Introduction

The formation of photochemical ozone occurs as a polluted urban air mass moves downwind during the day. In early modeling studies, a Lagrangian well-mixed chemical reactor was employed to investigate ozone chemistry as a function of time along the trajectory of the moving air mass (Hogo and Gery, 1988). The limitations of this approach included the possibly inaccurate location of the moving air mass resulting from accumulation of wind errors, overestimation of pollutant concentrations due to neglecting horizontal

*Corresponding author. Tel.: +1-509-335-5702; fax: +1-509-335-7632.

*E-mail address:* blamb@wsu.edu (B. Lamb).

1352-2310/03/$ - see front matter 
doi:10.1016/S1352-2310(02)01027-0

diffusion, and an inability to treat the specific distribution of sources across an urban airshed (Seinfeld and Pandis, 1998). To improve on this approach, the use of Eulerian grid models has become a common way to investigate ozone exceedances on urban and regional scales. The Urban Airshed Model (UAM) (Douglas et al., 1990), CALGRID (Yamartino et al., 1992), and, more recently, the Community Multi-scale Air Quality (CMAQ) model (Byun and Ching, 1999) are examples of the Eulerian approach that provides much more realism in the horizontal and vertical transport of precursors and products than was possible with a Lagrangian model. While these grid models allow relatively detailed treatment of the distribution of emissions within a modeling domain, it has been difficult to analyze ozone formation as a function of specific source areas and to investigate the evolution of photochemistry along downwind trajectories. Plume-in-grid methods have been developed to treat the evolution of plumes from specific large point sources until the plume reaches the scale of the horizontal grid (Byun and Ching, 1999). However, the plume-in-grid approach is not suited to document the detailed evolution of ozone formation along trajectories from urban centers to downwind rural receptors. In the last several years, a technique termed process analysis has been implemented in some grid models (Byun and Ching, 1999; Systems Application International, 1995) to determine the relative importance of different physical and chemical processes with respect to ozone formation within selected grids of the domain (Jang et al., 1995). As a diagnostic analysis tool, process analysis can be used to understand how the results of simulations are acquired. However, even in this case, it is difficult to determine the relationship between sources and receptors with respect to ozone formation within a moving air mass since the process analysis schemes are based upon fixed grid calculations. The most frequent application of process analysis is the investigation of the relative importance of different chemical production paths (Jang et al., 1995).

In this paper, we incorporate a process analysis scheme within the CALGRID model to investigate ozone formation patterns downwind of urban Seattle. We apply process analysis in two ways: first, we examine the role of chemistry, advection, diffusion and deposition within the grid cell where the maximum downwind ozone concentration occurs; second, we employ a simple approach using existing modeling tools to determine the back trajectory linking a downwind receptor to upwind source areas, and then we apply process analysis in a forward mode to the grids along the trajectory. The second approach yields quantitative information about the relative importance of diffusion, advection, deposition, and chemical production in changing ozone concentrations along the trajectory. The availability of these data provides additional information and a different perspective for understanding ozone concentration patterns that occur at different receptors downwind of an urban area. In fact, it becomes straightforward to examine changes in precursor concentrations and $VOC/NO_x$ ratios along the back trajectory simultaneously with the ozone process analysis.

In this paper, we employ this method to investigate the details of ozone formation within the Puget Sound area of western Washington State. The objective is to gain additional insight into ozone formation patterns in Puget Sound and to show how process analysis applied along the air mass transport path can help explain ozone behavior downwind of urban sources. The Puget Sound region has a history of periodic ozone episodes during the last twenty years, and recently has experienced considerable population growth and urban expansion. As a result, there is continued interest in improving our understanding of air pollutant behavior in the area. This interest provides the motivation for the current work as well as for the implementation and operation of a daily numerical air quality forecast system (http://airpact.wsu.edu/) that shares many of the attributes of the modeling system described in this paper. Since local agencies are using the forecast system as part of their air quality alert decision process, it is important to develop a good understanding of model performance and ozone formation patterns in the region.

## 2. Experimental methods

### 2.1. Description of the modeling system

Our investigation builds on work associated with the development and application of a regional modeling system for the Pacific Northwest that incorporates the Mesoscale Meteorological Model Version 5 (MM5) (Grell et al., 1995) with the CALMET/CALGRID (Scire et al., 1995; Yamartino et al., 1992) photochemical modeling pair and a detailed gridded emission inventory as described by Barna et al. (2000), Barna and Lamb (2000), and Barna et al. (2001). In these recent studies, the MM5 model was applied with three nested domains (grid cells size of 45, 15, and 5 km) to simulate meteorological fields over an inner domain that stretches from north of Vancouver, BC, to south of Portland, OR, and from west of the Pacific coastline to east of the crest of the Cascade Mountain range. In the work described by Barna and Lamb (2000), observations from 46 surface meteorological stations and two upper air stations were used in an observational nudging method within MM5 to improve the results of the wind field and subsequent ozone simulations. The MM5 wind fields were "passed through" the CALMET diagnostic wind model with minimal change and combined with the boundary layer scheme in CALMET

to provide winds and boundary layer parameters for direct use in the CALGRID photochemical model. The observational nudging analysis and resulting CALMET wind and boundary layer fields obtained in Barna and Lamb are used directly in the work described herein.

For this study, a smaller domain compared to that described by Barna and colleagues was used. The domain is shown in Fig. 1 and consists of 5 km × 5 km horizontal grid cells with 74 × 57 grids centered over downtown Seattle. There are 13 vertical layers with variable spacing. The first layer is 20 m deep and the top of the model domain is fixed at 5000 m.

We also updated the CALGRID model with the SAPRC-97 (Carter et al., 1997) kinetic chemical mechanism that includes explicit treatment of isoprene chemistry in place of the SAPRC-90 (Carter, 1990) mechanism used in the initial studies. We use uniform boundary concentrations for the model system. During this 11 July–14 July episode, winds were from the northwest into the domain and we took the north boundary as a reference for choosing boundary concentrations: 40 ppbC as total VOC, 1 ppbv $NO_x$, and 250 ppb CO (according to unpublished data collected by WSU and others near the north boundary areas in recent years). The proportions of individual VOC were determined using results of the simulations near the north boundary with a larger domain. The emission inventory employed in the earlier studies was updated by Puget Sound Clean Air Agency to account for some minor sources not included in the original work. A summary of the emission inventory for our domain is given in Table 1.

### 2.2. Incorporation of process analysis

The purpose of process analysis is to define the contribution of each of the chemical and physical processes to the total concentration change of certain species during a period of time within a specific grid. The processes that influence ozone formation and transport of ozone include chemical production, dry deposition,

Table 1
Emission budget for the 11–14 July 1996 episode, t/day

| Model species | Point sources | Area sources | Mobile sources | Biogenic sources |
|---|---|---|---|---|
| ALK1 | 8 | 78 | 96 | 37 |
| ALK2 | 8 | 47 | 24 | 0 |
| ARO1 | 6 | 25 | 27 | 0 |
| ARO2 | 3 | 21 | 21 | 0 |
| CCHO | 0 | 1 | 1 | 172 |
| CO | 241 | 681 | 2706 | 0 |
| ETHE | 0 | 7 | 8 | 0 |
| HCHO | 1 | 4 | 3 | 235 |
| ISOP | 0 | 0 | 0 | 309 |
| MEK | 2 | 10 | 1 | 149 |
| MGLY | 0 | 0 | 0 | 0 |
| NO | 95 | 76 | 223 | 37 |
| NO2 | 10 | 13 | 38 | 0 |
| OLE1 | 0 | 7 | 11 | 81 |
| OLE2 | 0 | 6 | 14 | 32 |
| OLE3 | 1 | 0 | 0 | 1333 |
| RCHO | 0 | 20 | 2 | 125 |
| Total VOC | 29 | 226 | 208 | 2474 |
| Total $NO_x$ as NO | 101 | 84 | 248 | 37 |
| VOC/$NO_x$ ratio | 1 | 6 | 2 | 144 |

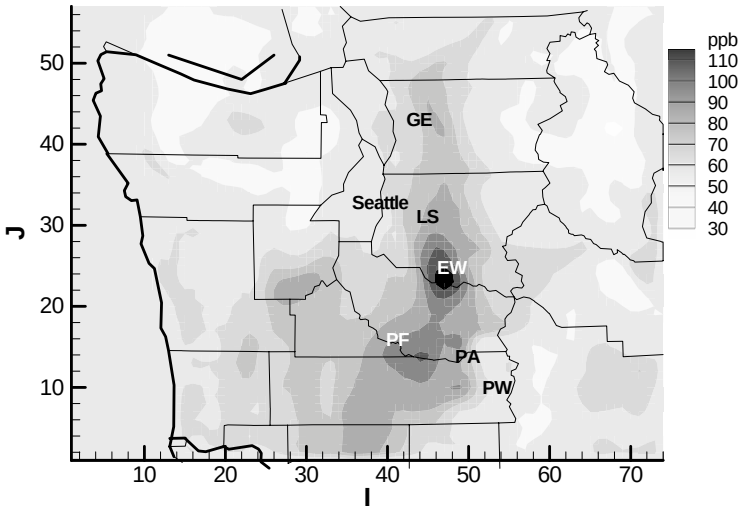


Fig. 1. Surface ozone concentration contour map, 15:00 PST on Sundy, 14 July 1996. Surface monitoring sites: Getchel (GE), Lake Sammamish (LS), Enumclaw (EW), Pack Forest (PF), Packwood (PW), and Paradise (PA).

horizontal advection and diffusion, and vertical advection and diffusion. For $NO_x$ and most of the VOC species, direct emissions must also be treated. The K-theory form of the atmospheric diffusion equation that is the basis for the CALGRID photochemical model is written as

$$\frac{\partial C_i}{\partial t} + U\frac{\partial C_i}{\partial x} + V\frac{\partial C_i}{\partial y} + W\frac{\partial C_i}{\partial z} = \frac{\partial}{\partial x}\left(K_x\frac{\partial C_i}{\partial x}\right) + \frac{\partial}{\partial y}\left(K_y\frac{\partial C_i}{\partial y}\right) + \frac{\partial}{\partial z}\left(K_z\frac{\partial C_i}{\partial z}\right) + R + D + S. \quad (1)$$

The first term on the left side is the change in concentration of species $i$ with time; the other three terms on the left side are the advection terms in $x$, $y$, and $z$ directions, and $U$, $V$ and $W$ are the mean wind speeds in the three directions, respectively. The first three terms on the right side are the turbulent diffusion terms, and $K_x$, $K_y$, and $K_z$ are turbulent diffusivities. The effects of chemical reactions ($R$), dry deposition ($D$), and emission sources ($S$) are included in the latter three terms on the right side. In a photochemical grid model, the set of simultaneous differential equations represented by Eq. (1) is integrated over time and space to determine the concentrations of precursor and product species at each grid point for each time step. Process analysis is used to find the contribution of each of these terms to the overall change of the concentration of the species concerned.

In this paper, process analysis is based on an internal 20 min time step used in the model, and the results are presented on an hourly basis. We modified the CALGRID source code to output $O_3$ concentration change due to chemical production, vertical advection/diffusion, dry deposition and horizontal advection/diffusion. We took advantage of operator splitting, inherent in the model structure, to make these process analysis computations. In CALGRID, the process analysis terms related to chemical production are calculated for each time step, while process analysis terms related to diffusion, advection and dry deposition are calculated every half time step. Given the relatively light winds that occurred during the modeling period, the internal time step provides sufficient resolution to calculate the contribution of each process with a reasonable degree of accuracy.

### 2.3. Calculation of back trajectories

In order to investigate ozone behavior in an air mass that affects a specific receptor, the back trajectory beginning at a specific time at the receptor must be obtained. To determine the back trajectory of an air mass transported through the model domain, it is important to employ the same meteorological fields as is used in the grid model. Since we are using CALMET to process the MM5 winds for input to CALGRID, a simple way to derive the location and timing of a back trajectory is to invert the CALMET wind fields and apply the companion CALPUFF Gaussian puff dispersion model (Scire et al., 2000) with a unit source strength. In this reverse diffusion mode, the centerline of the CALPUFF plume defines the back trajectory for the receptor of interest as illustrated in Fig. 2; information about the timing of upwind transport is also obtained. The back trajectory is based upon the three-dimensional CALMET wind field and includes any terrain effects as treated in CALMET. The contour lines obtained using CALPUFF in a reverse diffusion mode provide information about the probability that emissions from an upwind grid cell will impact a downwind receptor. However, for our purposes, the centerline of the reverse CALPUFF plume is used to identify grid cells and times for application of process analysis. Additional details are given in O'Neill et al. (2003), who have described the MM5/CALMET/CALPUFF system applied in this manner to map upwind source footprints for application to conserved chemical species (see, also, Napelenok et al., 2000).

## 3. Results

### 3.1. Ozone simulation results for the period of 11–14 July 1996

In this ozone episode, the domain peak ozone concentration occurred near Enumclaw about 40 km southeast of the Seattle urban center (Fig. 1). The observed and predicted time series of the six stations are shown in Fig. 3, and statistical model performance measures are summarized in Tables 2 and 3. At Getchel and Lake Sammamish that are within the I-5 urban corridor, the model overestimates nighttime ozone and shows reasonable agreement with daytime patterns. The nighttime overestimate is probably associated with $O_3$ titration by nighttime NO emissions into a shallow surface layer that does not appear to be correctly captured in the model. At Enumclaw, a rural site, the model shows excellent agreement with nighttime $O_3$ concentrations and also yields good agreement with daytime $O_3$ patterns. On Sunday when the maximum observed $O_3$ concentration reached 118 ppb, the model underestimated the peak by approximately 10% (106 ppb). At Paradise on the side of Mt. Rainier, the model predictions were in good agreement with peak daytime values and the timing of the peak was captured correctly. However, Paradise exhibits an elevated background concentration of ozone that increased from approximately 40 ppb on Thursday to 50 ppb by

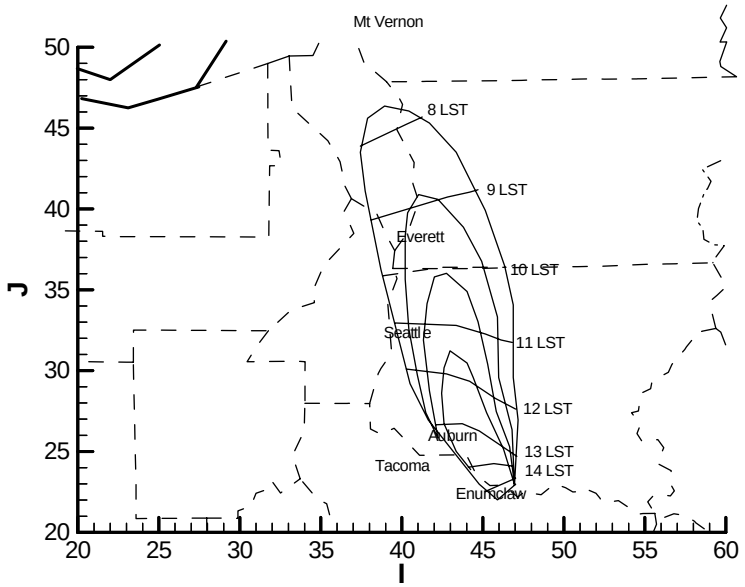


Fig. 2. Back trajectory plume contours from CALMET/CALPUFF applied in reverse diffusion mode originating at Enumclaw at 15:00 PST on Sunday, 14 July 1996.

Sunday. The model underestimates this increasing background by 10–20 ppb. At Pack Forest, another rural downwind site, the model underestimated peak daytime values during the first 2 days, but apparently overestimated observed values on Sunday. However, it should be noted that observations for all of Saturday and the first part of Sunday were missing for Pack Forest. At the third rural, downwind site, Packwood, the model exhibited overall general agreement with the observations. On three days, the model overestimated peak ozone concentrations, but at night, the model was in close agreement with the observations. These results and the statistical performance measures are similar to those reported by Barna and Lamb (2000); differences are attributed to the updated chemical mechanism, some corrections to the emission inventory provided by the Puget Sound Clean Air Agency, and revision of the boundary conditions for the smaller domain used in this study.

### 3.2. Single grid process analysis

Since the domain peak ozone appeared at Enumclaw, we have chosen this site to do the process analysis for the 11–14 July 1996 episode. The results of process analysis include the hourly time series of chemical production, vertical advection/diffusion, horizontal advection/diffusion, and dry deposition for each specified grid cell. Figs. 4a–c show the results of 20 m surface layer process analysis for the Enumclaw grid cell on Sunday, 14 July 1996. Process analysis applied to the moving air mass arriving at Enumclaw in mid-afternoon is described in a later section. In general, ozone concentrations in the first layer are enhanced by the vertical advection/diffusion of ozone-rich air from aloft and depleted by dry deposition processes at the surface as shown in Fig. 4a. In CALGRID, dry deposition rates are calculated using a resistance-based scheme. The results show that dry deposition can be as high as 200 ppbv/h, but most of the dry deposition loss is counteracted by vertical diffusion from layers aloft. As a result, the net effect of vertical transport and deposition is similar in magnitude to the other terms as shown in Fig. 4b where vertical transport has been combined with dry deposition into a single vertical process term.

During the nighttime period from midnight to about 06:00, there is a slow net removal of ozone within the grid at −1 to −2 ppbv/h. This is due to a small rate of chemical loss (−1 ppbv/h) and slightly more removal due to the vertical term (0 to −11 ppbv/h) compared to the positive contribution of horizontal transport (0–10 ppbv/h). After sunrise, the net change in grid ozone concentration exhibits a relatively steady rate at approximately 10 ppbv/h. This increase in ozone within the grid cell is due to a steady increase in the rate of ozone chemical production that peaks at 20 ppbv/h in mid-afternoon. During this period, the vertical term is small, but mostly positive (−2 to 2 ppbv/h), while the horizontal transport term varies from 6 ppbv/h at 10:00 to −8 ppbv/h from noon to 15:00. At mid-afternoon when the chemical production peaks and then begins a steady decline, the net rate of change in ozone exhibits a rapid decrease from 12 ppbv/h at 14:00 to −15 ppbv/h at 16:00. This change is due to the decrease in ozone

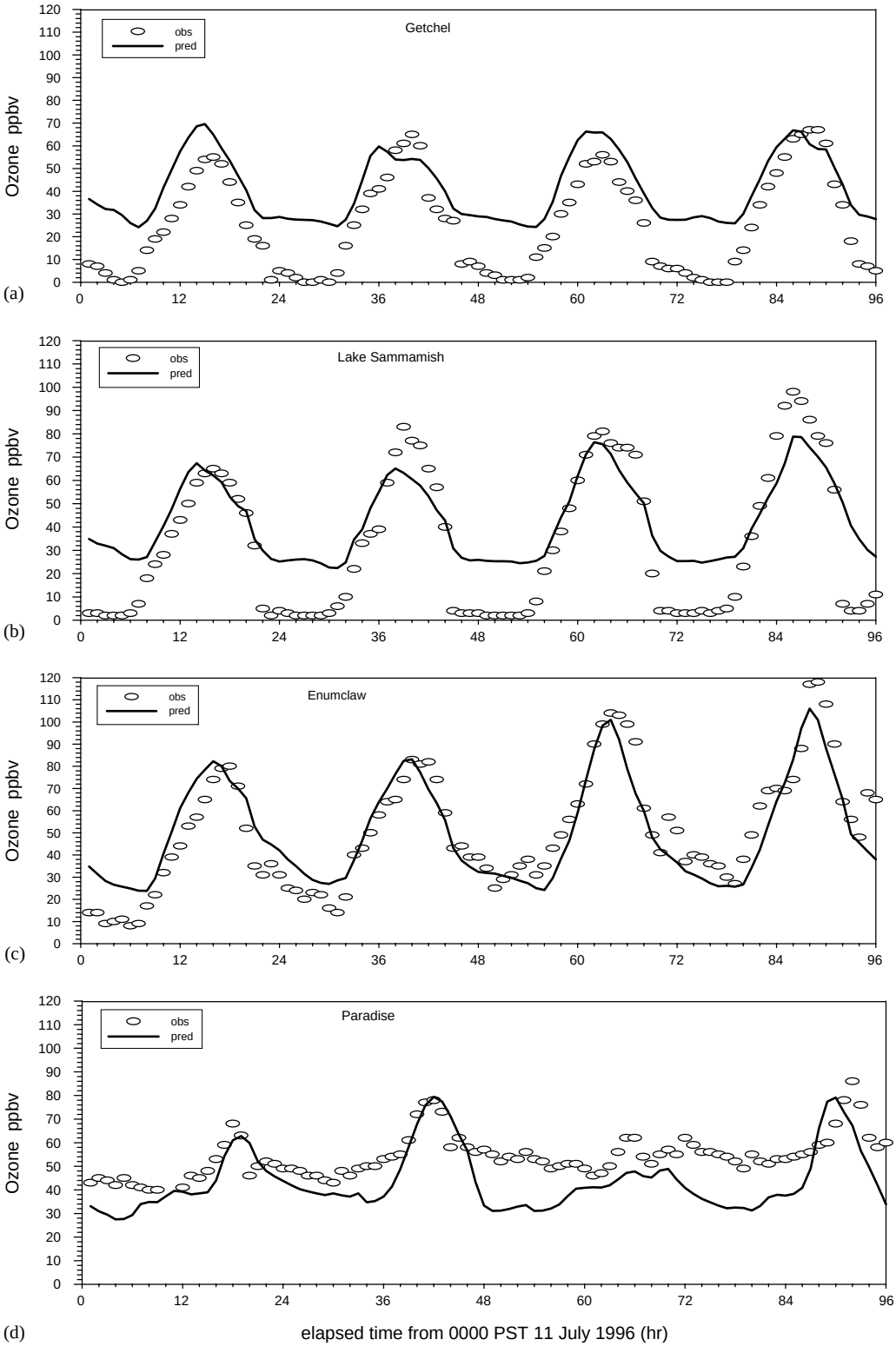


Fig. 3. Time series of observed and predicted ozone concentrations at the Puget Sound monitoring sites: (a) Getchel, (b) Lake Sammamish, (c) Enumclaw, (d) Paradise, (e) Pack Forest and (f) Packwood.

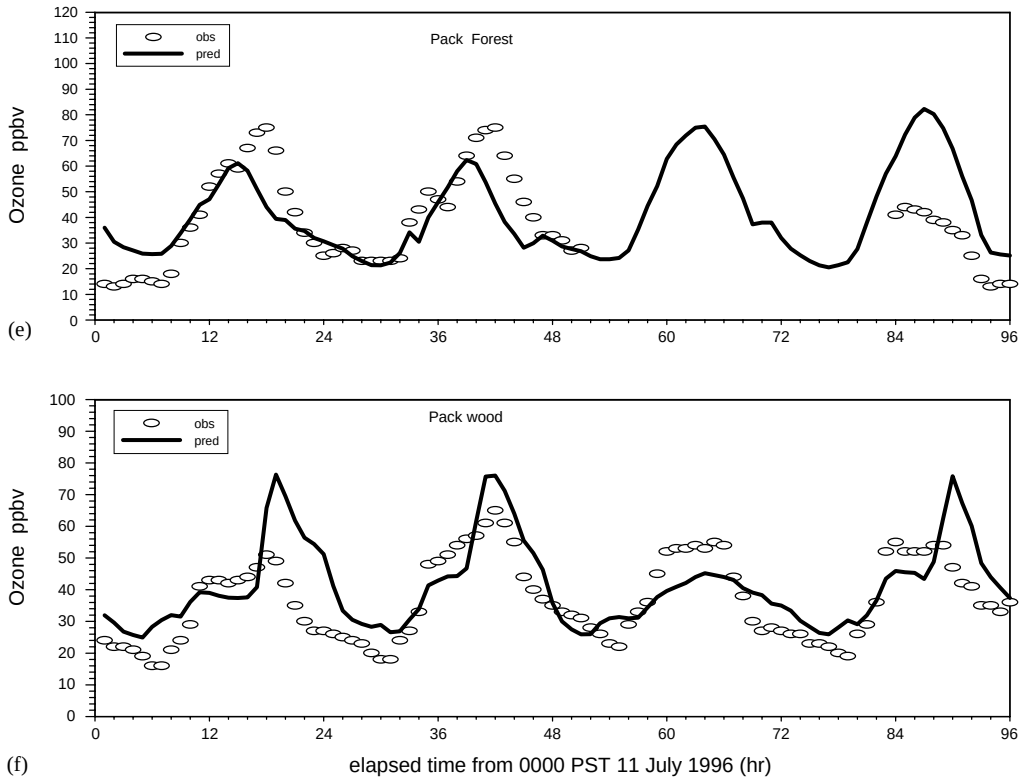


Fig. 3 (*continued*).

Table 2
Summary of model performance statistics for the 11–14 July 1996 episode in Puget Sound

| Monitor | Enumclaw | Getchel[a] | Lake Sammamish[a] | Paradise | Pack forest | Packwood |
|---|---|---|---|---|---|---|
| Avg obs $O_3$ (ppb) | 55.4 | 40.9 | 57.6 | 56.0 | 37.8 | 38.2 |
| Avg pred $O_3$ (ppb) | 51.2 | 50.0 | 54.5 | 44.5 | 42.2 | 40.9 |
| Std. dev. obs $O_3$ (ppb) | 25.9 | 16.3 | 24.4 | 8.6 | 16.3 | 13.2 |
| Std. dev. pred $O_3$ (ppb) | 23.7 | 12.2 | 15.2 | 13.6 | 18.9 | 12.8 |
| Slope | 0.85 | 0.66 | 0.58 | 1.2 | 0.56 | 0.74 |
| Intercept (ppb) | 4.3 | 23.1 | 21.0 | -22.3 | 20.9 | 12.6 |
| Rmsd (ppb) | 10.5 | 12.1 | 11.7 | 14.6 | 18.3 | 9.3 |
| Model index | 0.95 | 0.83 | 0.91 | 0.63 | 0.65 | 0.86 |
| Normalized gross error (%) | 18.8 | 37.1 | 25.5 | 23.7 | 37.5 | 22.1 |
| Normalized bias (%) | −3.4 | 33.7 | 8.8 | −21.2 | 20.9 | 11.8 |
| 14 July 1996 max obs $O_3$ ppb | 118 | 67 | 98 | 86 | No data | 55 |
| 14 July, 1996 max pred $O_3$ ppb | 106 | 67 | 79 | 79 | | 76 |

[a] Nighttime $O_3$ concentrations less than 10 ppb excluded.

production rate coupled with a dramatic loss of ozone due to horizontal transport that reaches −28 ppbv/h at 16:00. It should be noted that loss due to horizontal transport can occur due to relatively ozone poor air advected into the cell or relatively ozone rich air advected out of the cell. Given the high concentrations that occurred during the afternoon, the loss due to horizontal transport probably represents removal of ozone-rich air from the cell. During this period of rapid change in these process terms, the vertical transport/deposition term remains small between −2 and 2 ppbv/h. As sunset approaches from 18:00 to 21:00, the net

Table 3
Summary of overall model performance statistics for Puget Sound and comparison to results from Barna and Lamb (2000) and to results for UAM-V and SMRAQ applications to the northeastern US (Hogrefe et al., 2001)

| Performance measure | This work | Barna and Lamb (2000) | UAM-V | SMRAQ | EPA guidelines |
|---|---|---|---|---|---|
| Overall slope | 0.68 | 0.65 | na | na | na |
| Overall intercept (ppb) | 14.1 | 13.9 | na | na | na |
| Overall correlation coefficient | 0.78 | 0.65 | 0.66 | 0.52 | na |
| Overall normalized gross error (%) | 25.8 | 24.0 | 20.0 | 23.0 | Within 35% |
| Overall normalized bias (%) | 5.0 | -9.8 | 6 | 8 | ±15% |

na: not available

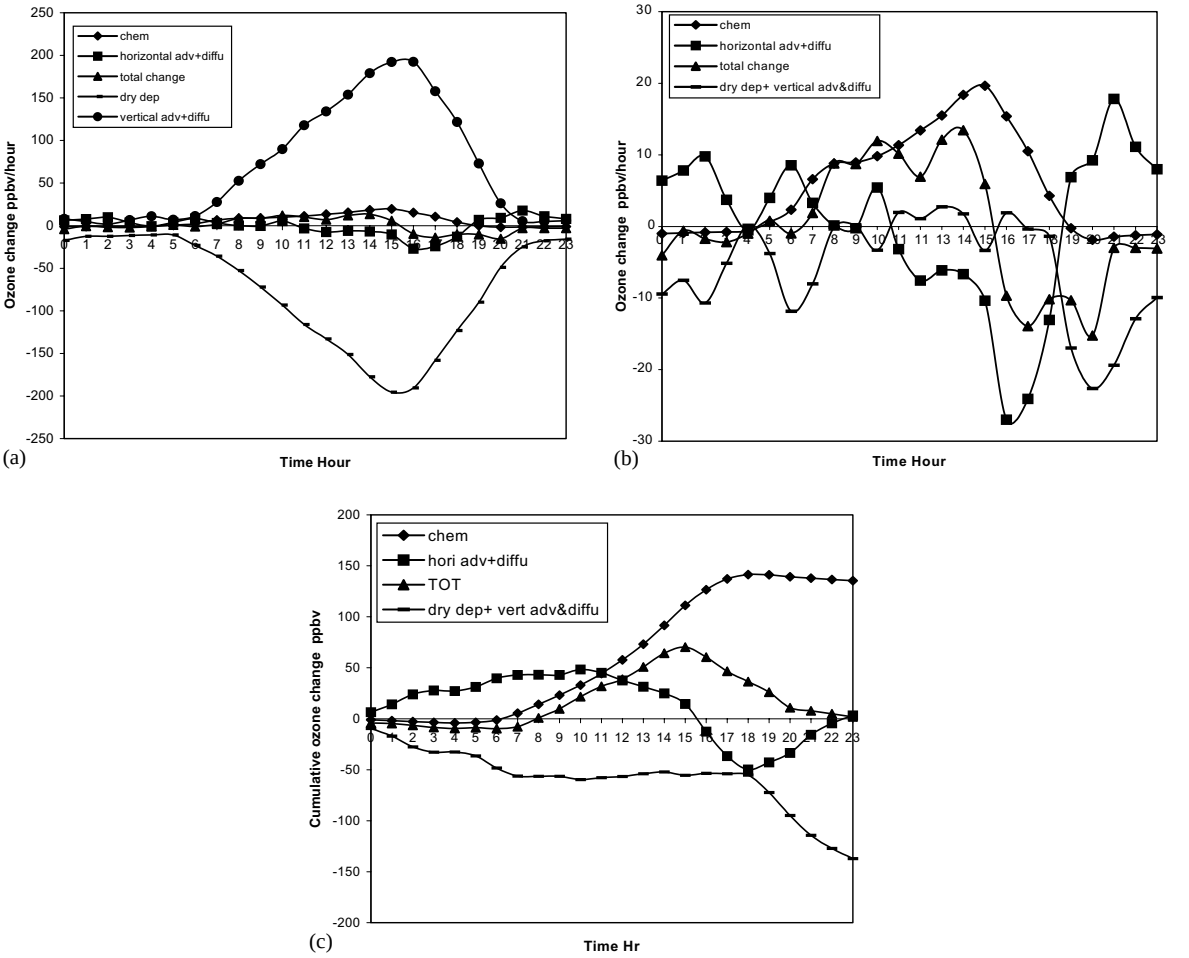


Fig. 4. (a) Hourly change in ozone concentration within the Enumclaw grid cell calculated from process analysis using the CALGRID model during Sunday, 14 July 1996. (b) Hourly change in ozone concentration within the Enumclaw grid cell calculated from process analysis using the CALGRID model during Sunday, 14 July 1996. Vertical transport and dry deposition are combined in a single vertical term. (c) Cumulative change in ozone concentration within the Enumclaw grid cell calculated from process analysis using the CALGRID model during Sunday, 14 July 1996. Vertical transport and dry deposition are combined in a single vertical term.

change in ozone within the grid cell remains negative at approximately −13 ppbv/h due primarily to an increase in removal associated with the vertical transport/deposition term. The effects of horizontal transport switch from negative to positive during this period. During the remainder of the night, the patterns return to

those of the previous night with a small net loss of ozone due to the combination of chemical removal and vertical transport/deposition offset by a positive contribution from horizontal transport.

The cumulative change in ozone of each term during the day indicates the overall effect of ozone formation and transport that occurred in the grid cell. As shown in Fig. 4c, the total cumulative change in ozone was small (2 ppbv) and consistent with the nearly identical ozone concentrations that existed at the beginning and end of the 24 h period. The integrated chemical production rate was 136 ppbv during 24 h, but this was countered by the cumulative net vertical diffusion and dry deposition rate of −137 ppbv during 24 h. The horizontal advection cumulative term was very small (3 ppbv) compared to the large chemical production and vertical transport terms. At 15:00, when the total accumulative changes in ozone reached a maximum value (70 ppbv), the cumulative chemical production was the dominate contributing term (111 ppbv) and the combined cumulative dry deposition and vertical diffusion was the only negative term (−55 ppbv). The cumulative horizontal advection at mid-afternoon was relatively small (14 ppbv).

This grid cell specific process analysis shows that on a local basis in the model, the occurrence of high ozone concentrations during the day are the result of an imbalance between high local chemical production rates and dry deposition. After the peak concentration occurs, ozone is removed from the grid cell due to horizontal transport, and at night ozone is continually lost at a low rate due to chemical removal and vertical deposition. In the next section, we investigate how Enumclaw is affected by ozone changes along the trajectory from urban Puget Sound arriving at Enumclaw in mid-afternoon.

### 3.3. Process analysis applied to a moving air mass

In the episode under consideration, the peak ozone concentration was higher in the modeling domain on weekend days compared to weekdays, in spite of the fact that urban $NO_x$ and VOC emissions were lower on the weekend compared to weekdays. It is of interest to analyze ozone formation and transport on these different types of days. The transport and formation of ozone during the afternoon hours on Friday, 12 July, and Sunday, 14 July, were similar in two aspects. First, the air masses that reached the Enumclaw receptor traveled along similar trajectories over and downwind of the Seattle urban core. Second, on both days, ozone at Enumclaw increased from the early morning hour and reached maximum levels at 15:00 LST. However, on Friday, the peak level predicted was 83 ppbv and on Sunday, the peak level predicted was 106 ppbv. The corresponding observed concentrations were 80 ppbv on Friday and 118 ppbv on Sunday.

To determine why the peak ozone concentration was much higher on Sunday compared to Friday, we apply process analysis in a forward mode to each grid cell along the appropriate trajectory for the time that the air mass passed through the grid cell. The reverse CALPUFF plumes originating at Enumclaw at 15:00 LST on Friday are shown in each panel of Figs. 5 and 6 and for Sunday in each panel of Figs. 7 and 8. We retrieved process analysis results for each grid cell lying along or near the centerline of the reverse CALPUFF plumes for each day. The results are shown in Table 4 in terms of

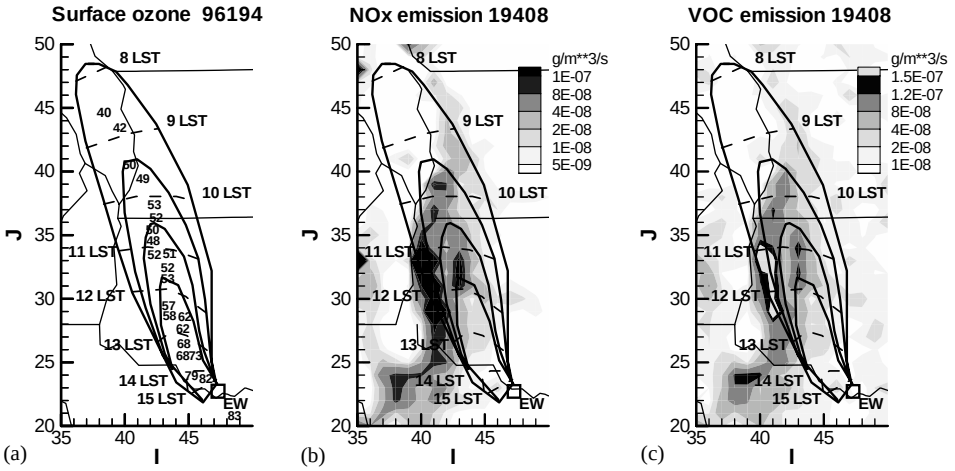


Fig. 5. (a)–(c) Map of back trajectory reverse CALPUFF plume originating at Enumclaw at 15:00 PST on Friday, 12 July 1996 with (a) ozone concentrations for indicated times and locations along the trajectory, (b) underlying 08:00 PST $NO_x$ emissions and (c) underlying 08:00 anthropogenic VOC emissions.

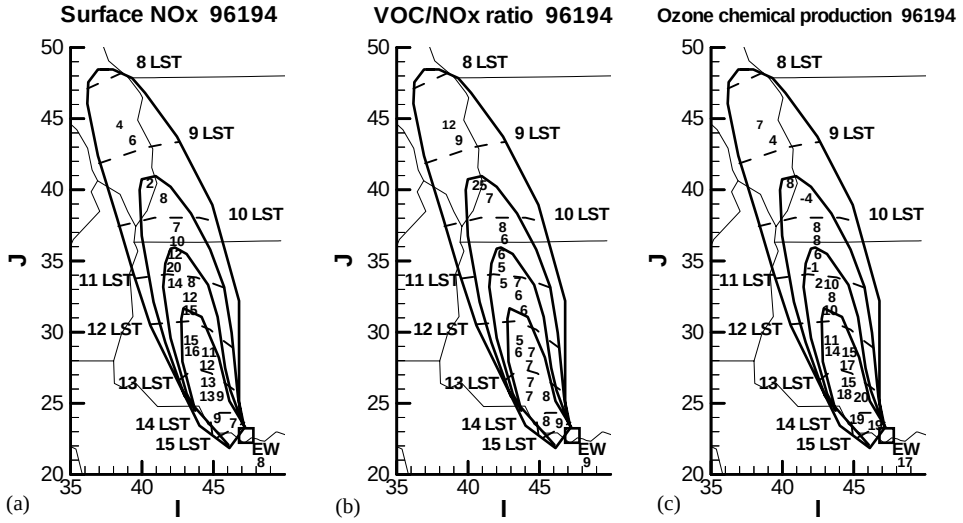


Fig. 6. (a)–(c) Map of back trajectory reverse CALPUFF plume originating at Enumclaw at 15:00 PST on Friday, 12 July 1996 with (a) $NO_x$ concentrations, (b) VOC/$NO_x$ ratios, and (c) $O_3$ chemical production rates for indicated times and locations along the trajectory.

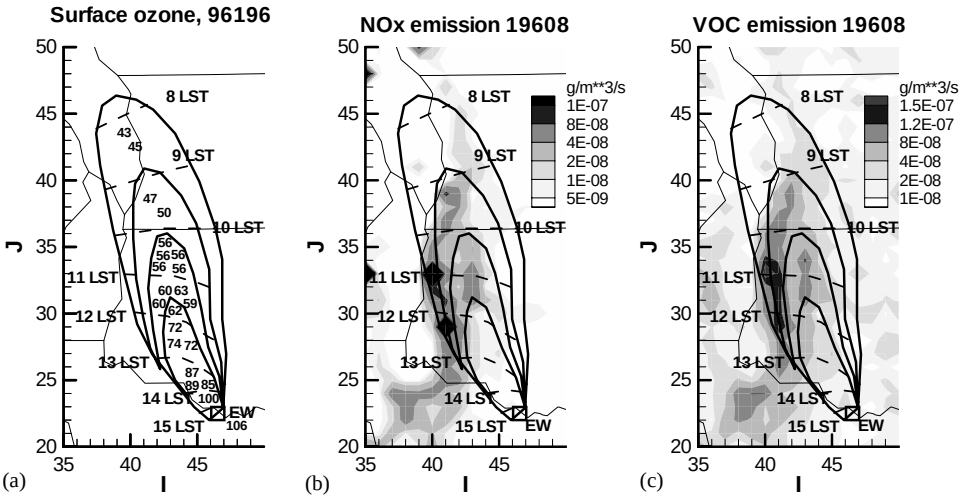


Fig. 7. (a)–(c) Map of back trajectory reverse CALPUFF plume originating at Enumclaw at 15:00 PST on Sunday, 14 July 1996 with (a) ozone concentrations for indicated times and locations along the trajectory, (b) underlying 08:00 PST $NO_x$ emissions and (c) underlying 08:00 anthropogenic VOC emissions.

the hourly averaged chemical production, vertical transport/deposition, and horizontal advection calculated by averaging the corresponding values of the grid cells within the hour lines in the back trajectory as shown in Figs. 5–8.

For both days, chemical production rates were small initially and then increased to maximum levels by approximately 13:00 to 14:00 LST. Contributions from vertical diffusion and deposition were initially positive, then switched to negative at 10:00 LST, increased to maximum levels between 12:00 and 13:00 LT, and finally decreased to lower negative rates after 14:00–15:00 LST. Horizontal advection provided negative contributions early and again late in the trajectory and relatively small positive contributions during the middle of the day.

It is most useful to examine the total effect of each process for each day. The total change in ozone concentration along the trajectory due to chemical

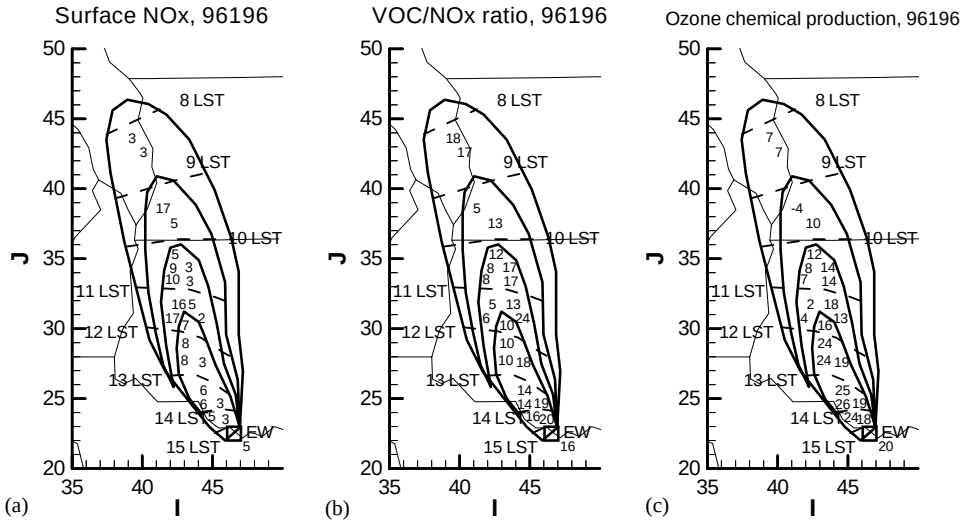


Fig. 8. (a)–(c) Map of back trajectory reverse CALPUFF plume originating at Enumclaw at 15:00 PST on Friday, 12 July 1996 with (a) $NO_x$ concentrations, (b) VOC/$NO_x$ ratios, and (c) $O_3$ chemical production rates for indicated times and locations along the trajectory.

production was 87.9 ppb for Friday and 118.3 ppb for Sunday. The total vertical diffusion and dry deposition for the 2 days were −35.6 and −49.7 ppb, which represents approximately 40% of the net chemical production effect on both days. The net horizontal advection terms for the 2 days were relatively small at approximately 12% of chemical production on Friday and 4% of chemical production on Sunday. This analysis shows that chemical production of ozone along the transport path leads to a net increase in ozone in the air mass and that the chemical production rate on Friday was smaller than on Sunday. At the same time, deposition losses were a consistent fraction of the net chemical production rate and horizontal effects were small. The latter is consistent with the fact that our analysis seeks to treat a moving air mass where advection effects should be minimal.

It is worth examining other aspects of the model simulation in the context of the back trajectory process analysis results. First, as shown in Table 4, the net ozone change for Friday and Sunday was 41.4 and 64.1 ppbv, respectively. As shown in Figs. 5a and 7a, the initial $O_3$ concentration at 08:00 upwind of Puget Sound was 41 ppbv for Friday and 44 ppbv for Sunday. Adding the net change to these initial values yields peak ozone concentrations at Enumclaw at 15:00 LST equal to 82.4 ppb for Friday and 108.1 ppb for Sunday. These values are in very good agreement with the model output results of 83 and 106 ppb for Friday and Sunday, respectively. The very small differences between the peak ozone levels calculated along the back trajectory and those simulated from CALGRID, and the small contribution of horizontal advection along the back trajectory confirm that application of process analysis is consistent with the grid model simulation as expected.

Given that there are obvious differences in ozone production between Friday and Sunday for this episode, we investigate why these differences occur. All along the back trajectory, as shown in Fig. 5a and 7a, the ozone increase on Sunday was higher than on Friday during the same hours of the day. From 09:00–10:00 on both Friday and Sundy, the ozone level was about 50 ppbv. After 10:00, the rates at which ozone increased on Sunday were obviously higher than the corresponding period on Friday. On Sunday at 11:00, the ozone concentration was about 62 ppbv, while on Friday at the same time, the ozone concentration was only 52 ppbv. In the following hours, the higher rates of ozone production on Sunday resulted in much higher ozone concentration in mid-afternoon compared to Friday.

$NO_x$ and VOC emissions are higher on the weekdays than in weekend days due to more mobile source emissions during weekdays. With similar mixed layer heights, higher $NO_x$ and VOC concentrations can be expected on 12 July compared to the 14th. As shown in Fig. 6a and Fig. 8a, modeled $NO_x$ concentrations were higher on 12 July than on 14 July. The $NO_x$ levels between 10:00 and 15:00 on 12 July ranged from 7 to 20 ppbv and most of the time they were greater than 10 ppbv. On 14 July, they ranged from 2 to 17 ppbv, and most of the time they were less than 10 ppbv. However, high $NO_x$ and VOC concentrations do not necessarily lead to high chemical production rates, since chemical production rate depends not only on ambient $NO_x$ and VOC concentrations, but also on VOC/$NO_x$ ratios. In this episode, VOC/$NO_x$ ratios were generally low within

Table 4
Summary of process analysis results along the air mass trajectory for Friday, 12 July and Sunday, 14 July in Puget Sound

| 12 July time PST | Chemical production (ppbv/h) | Dry deposition and vertical diffusion (ppbv/h) | Horizontal advection (ppbv/h) | Net change (ppbv/h) | 14 July time PST | Chemical production (ppbv/h) | Dry deposition and vertical diffusion (ppbv/h) | Horizontal advection (ppbv/h) | Net change (ppbv/h) |
|---|---|---|---|---|---|---|---|---|---|
| 08 | 5.6 | 7.2 | −8.7 | 4.1 | 08 | 7.0 | 5.2 | −6.5 | 5.7 |
| 09 | 2.0 | 6.9 | −1.3 | 7.6 | 09 | 3.2 | 3.4 | −1.3 | 5.3 |
| 10 | 5.2 | −3.2 | 7.4 | 9.4 | 10 | 11.0 | −4.0 | 0.1 | 7.2 |
| 11 | 7.2 | −4.9 | 4.4 | 6.7 | 11 | 10.6 | −7.5 | 3.8 | 6.9 |
| 12 | 14.2 | −11.9 | 4.4 | 6.7 | 12 | 22.1 | −18.3 | 5.6 | 9.3 |
| 13 | 17.7 | −13.4 | 1.2 | 5.5 | 13 | 23.5 | −22.5 | 10.5 | 11.5 |
| 14 | 19.1 | −7.6 | −7.7 | 3.8 | 14 | 21.1 | −2.6 | −6.4 | 12.1 |
| 15 | 16.8 | −8.5 | −10.6 | −2.4 | 15 | 19.7 | −3.4 | −10.4 | 5.9 |
| Total change | 87.9 | −35.6 | −10.9 | 41.4 | | 118.2 | −49.7 | −4.5 | 64.1 |

Table 5
Peak ozone levels on Friday, 12 July, and Sunday, 14 July, predicted for different combinations of emission and meteorology

| | Friday meteorology (ppbv) | Sunday meteorology (ppbv) | Meteorology effect (ppbv) |
|---|---|---|---|
| Friday emissions | 83 | 89 | 6 |
| Sunday emissions | 96 | 106 | 10 |
| Emissions effect | 13 | 17 | |

the source regions and along the path that the air masses traveled through to reach Enumclaw at around 15:00. Although $NO_x$ concentrations were higher on 12 July than on 14 July along the trajectory, VOC/$NO_x$ ratios were lower and so was the chemical production rate. As shown in Fig. 6b and Fig. 8b, between 10:00 and 15:00 LST, VOC/$NO_x$ ratios on 14 July ranged from 5 to 20 and, most of the time, the ratio was greater than 10. The chemical production rate ranged from 2 to 26 ppbv/h and most of the time the production rate was greater than 14 ppbv/h (Fig. 8c). On 12 July, the VOC/$NO_x$ ratio ranged from 5 to 9, chemical production rate ranged from −1 to 20 ppbv/h and no more than 10 ppbv/h in the first 2 h of this period (Fig. 6c). In these two cases, it appears that the VOC/$NO_x$ ratio has a key role in determining the ozone production rate. As shown in Table 1, the average VOC/$NO_x$ ratio in the emission inventory on the domain scale is about 2 for mobile emissions, 6 for anthropogenic source emissions, 144 for biogenic source emissions and 1 for point source emissions. The anthropogenic area emissions, biogenic emissions and point source emissions remain almost the same as on weekdays and during the weekend. Thus, lower mobile emissions on the weekend lead to increases in VOC/$NO_x$ ratios in the domain. Blanchard and Fairley (2001) found the similar trend of ozone levels in the central California area. In their simulations, weekend levels of $NO_x$ were significant lower than weekday, but in the sites with relatively low VOC emissions, weekend ozone levels tended to be higher than weekday levels.

To further test the effects of different emission patterns on Friday versus Sunday, we re-ran the simulations and used Sunday emissions with the meteorological fields from Friday and vice versa. The predicted peak ozone concentrations at Enumclaw are listed in Table 5 for each combination of emissions and meteorology. The effects of weekday versus weekend emissions increased the peak ozone concentration by 13 and 17 ppbv using Friday and Sunday meteorology, respectively. For comparison, the effects of different meteorology produced differences in peak ozone concentrations of 6 and 10 ppbv on Friday and

Sunday, respectively. These results indicate that the higher peak ozone level on Sunday is related to both emissions and meteorology. However, the effects of weekend emissions produced about twice the increase in peak ozone compared to the effects of meteorology.

### 3.4. Summary and conclusions

To investigate the details of ozone formation and evolution in the Puget Sound region of Washington state, a process analysis scheme was incorporated into a regional Eulerian grid model and applied for a single grid at Enumclaw where the peak ozone concentration occurred and also along a back trajectory from Enumclaw to the upwind urban core. On a local basis, the process analysis results showed that steady increase in chemical production of ozone during the day exceeded vertical and horizontal removal rates and led to peak ozone concentrations during mid-afternoon. Following this period of peak ozone concentration, horizontal advection had a large impact upon ozone removal from the cell. At night, deposition coupled with chemical loss led to a net removal of ozone, while horizontal advection effects were variable. We used the CALPUFF dispersion model in a reverse diffusion mode to define the back trajectory, and then applied process analysis in a forward mode to grids along the trajectory. These results show that chemical production along the trajectory exceeded vertical transport/deposition and horizontal advection effects after approximately 10:00 LST. We used these results to examine differences in ozone formation on Friday when peak ozone levels reached 80 ppbv in comparison to ozone formation on Sunday when peak ozone levels reached 118 ppbv observed. Formation of peak ozone in Enumclaw was due to ozone chemical production and accumulation on a continuous basis from the early morning through the mid-afternoon until the air mass reached the receptor. Peak ozone differences between 12 July, Friday and 14 July, Sunday were principally due to the differences in ozone production rates along the trajectory to the Enumclaw monitoring site. In turn, the differences in ozone production rates on the 2 days were related to both emission and meteorology. Lower mobile emissions on the weekend led to higher VOC/$NO_x$ ratios and thus higher chemical production rates on weekend days compared to weekdays. Grid model simulations with Friday emissions used with Sunday meteorological fields and vice versa confirmed that emissions had a larger effect on the peak ozone for the 2 days compared to meteorology.

Process analysis is a relatively new approach in photochemical air quality modeling. Currently, only a few photochemical systems have such options. These model systems include CMAQ (Byun and Ching, 1999), UAM-V (Systems Application International (SAI), 1995), and CAMx (Environ International Corporation, 2002); Pottier et al. (2000) used the process analysis function of UAM-V to define the contributions of physical and chemical processes to ozone formation and consumption. Our study shows how process analysis can help provide new insight into ozone formation and how it can be used to investigate local effects at a single grid and also ozone evolution along an air mass transport path.

## References


Barna, M., Lamb, B., 2000. Improving ozone modeling in regions of complex terrain using observational nudging in a prognostic meteorological model. Atmospheric Environment 34, 4889–4906.

Barna, M., Lamb, B., O'Neill, S., Westberg, H., Figueroa-Kaminsky, C., Otterson, S., Bowman, C., 2000. Modeling ozone formation and transport in the Cascadia region of the Pacific Northwest. Journal of Applied Meteorolgy 39, 349–366.

Barna, M., Lamb, B., Westberg, H., 2001. Modeling the effect of VOC/$NO_x$ emissions on ozone synthesis in the Cascadia airshed of the Pacific Northwest. Journal of Air and Waste Management Association 51, 1021–1034.

Blanchard, C.L., Fairley, D., 2001. Spatial mapping of VOC and $NO_x$-limitation of ozone formation in central California. Atmospheric Environment 35, 3861–3873.

Byun, D.W., Ching, J.K.S., 1999. Science algorithms of the EPA Models-3 Community multiscale air quality (CMAQ) modeling system, EPA/600/R-99/030.

Carter, W.P.L., 1990. A detailed mechanism for the gas-phase atmospheric reactions of organic compounds. Atmospheric Environment 24A, 481–510.

Carter, W.P.L., Luo, D., Malkina, I.L., 1997. Environmental chamber studies for development of an updated photochemical mechanism for VOC reactivity assessment. Final Report to California Air Resources Board, Contract 92-345, Coordinating Research Council, Inc., Project M-9, 219 Atlanta, GA.

Douglas, S.G., Kessler, R.C., Carr, E.L., 1990. User's guide for the Urban Airshed Model, Vol. III: User's manual for the diagnostic wind model, Report No. EPA-450/4-90-007C, US Environmental Protect Agency, Research Triangle Park, NC.

Environ International Corporation, 2002. User's guide to comprehensive air quality model with extensions (CAMx). Version 3.10, Environ International Corporation, Novato, CA.

Grell, G.A., Dudhia, J., Stauffer, D.R., 1995. A description of the fifth-generation Penn State/NCAR mesoscale model (MM5). Report No. NCAR/TN-398 + STR, National Center for Atmospheric Research, Boulder, CO.

Hogo, H., Gery, M.W., 1988. Users guide for executing OZIPM-4 with CBM-IV or optional mechanism. Vol. 1. Description of the ozone isopleth plotting package-version 4, EPA/600/8-88/073a, US EPA, Research Triangle Park, NC.

Hogrefe, C., Rao, S.T., Kasibhatla, P., Hao, W., Sistla, G., Mathur, R., McHenry, J., 2001. Evaluating the performance

of regional-scale photochemical modeling systems: Part II-ozone predictions. Atmospheric Environment 35, 4175–4188.

Jang, J.C., Jeffries, H.E., Tonnesen, S., 1995. Sensitivity of ozone to model grid resolution—II. Detailed process analysis for ozone chemistry. Atmospheric Environment 29, 3101–3114.

Napelenok, S., O'Neill, S.M., Lamb, B.K., Allwine, E.J., Stock, D., 2000. Modeling the upwind pollutant source footprint along backward trajectories using the MM5/CALMET/CALPUFF modeling system. Third Urban Symposium. American Meteorological Society, Davis, CA.

O'Neill, S.M., Lamb, B.K., Chen, J., Napelenok, S., Allwine, E.J., McManus, D.S.J.B., Shorter, J.H., Kolb, C.E., 2003. Correlating an upwind source-footprint with urban emissions data using the MM5/MCIP/CALPUFF modeling system. Atmospheric Environment, submitted for publication.

Pottier, J.L., Deuel, H.P., Pryor, S.C., 2000. Application of the UAM-V and use of indicator species to assess control strategies for ozone reduction in the Lower Fraser Valley of British Columbia. Environmental Monitoring and Assessment 65, 459–467.

Scire, J.S., Insley, E.M., Yamartino, R.J., Fernau, M.E., 1995. A user's guide for the CALMET meteorological model. Earth Tech, Concord, MA.

Scire, J.S., Strimaitis, D.G., Yamartino, R.J., 2000. A user's guide for the CALPUFF dispersion model (Version 5). Earth Tech, Concord, MA.

Seinfeld, J.H., Pandis, S.N., 1998. Atmospheric Chemistry and Physics. Wiley, New York.

Systems Application International, 1995. User's guide to the variable grid urban airshed model (UAM-V). SYSAPP-99-95/27r2, Systems Applications International, San Rafael, CA.

Yamartino, R.J., Scire, J.S., Carmichael, G.R., Chang, Y.S., 1992. The CALGRID mesoscale photochemical grid model I. Model formulation. Atmospheric Environment 26A, 1493–1512.